

ACOUSTIC GAS THERMOMETRY

¹M. R. Moldover, ²R. M. Gavioso, ³J. B. Mehl, ⁴L. Pitre, ⁵M. de Podesta, ⁶J. T. Zhang.

¹Sensor Science Division, National Institute of Standards and Technology, Gaithersburg, MD, USA

²Thermodynamics Division, Istituto Nazionale di Ricerca Metrologica, 10135 Turin, Italy

³36 Zunuqua Trail, PO Box 307, Orcas, WA 98280-0307, USA

⁴Laboratoire Commun de Métrologie LNE-CNAM (LCM), 61 rue du Landy, 93210 La Plaine Saint-Denis, France

⁵National Physical Laboratory, Teddington, Middlesex, TW11 0LW, UK

⁶National Institute of Metrology, Beijing 100013, China

1. Introduction: Overview Acoustic Gas Thermometry (AGT)

This appendix has a high information density and includes 60+ references to the archival literature. Many of the details in this appendix and many references will not be helpful during a first reading about AGT. We suggest that an overview of AGT can be found in four references: (1) Moldover *et al.* (1988) describe the theory and measurement of the acoustic resonances of a gas-filled spherical cavity. (2) Benedetto *et al.* (2004) thoroughly discuss relative primary AGT and they include a compact list of the corrections to the acoustic resonance frequencies. (3) Zhang *et al.* (2011) provide a similar list of acoustic corrections for a gas-filled cylindrical cavity. (4) Pitre *et al.* (2011) explain clearly how they used microwave resonances to determine the volume of a quasi-spherical cavity.

1.1. Overview of Absolute Primary AGT

Absolute primary AGT exploits the relationship between the speed of sound in a dilute gas u^2 and the thermodynamic temperature T and pressure p of the gas

$$u^2 = \left(\frac{\partial p}{\partial \rho} \right)_S = \frac{\gamma_0 k_B T}{m} + A_1(T)p + A_2(T)p^2 + \dots \quad (1)$$

In Eq. (1), ρ is the mass density of the gas; S is the entropy; $\gamma_0 \equiv C_p^0/C_v^0$ is the zero-density ratio of the constant-volume specific heat to the constant-pressure specific heat that is exactly 5/3 for the monatomic gases; k_B is the Boltzmann constant, and m is the average mass of an atom or molecule in the gas. Exact thermodynamic relationships connect $A_1(T)$ and $A_2(T)$ to the density virial coefficients and their temperature derivatives. [Trusler (1991); Gillis and Moldover (1996)] For AGT, the speed of sound in monatomic gases has been accurately determined by measuring the acoustic resonance frequencies of gas-filled cavities enclosed by heavy metal walls such as those shown in Fig. 1.

The first equality in Eq. (1) was derived from the linearized Navier-Stokes equations which are themselves derived from the Boltzmann equation. Corrections to this equality resulting from the non-zero amplitude of sound [Hamilton *et al.* (2001); Coppens and Sanders (1968)] and the non-zero frequency of sound [Greenspan (1956)] are known; they are negligible at the acoustic amplitudes, gas densities, and acoustic frequencies used for AGT. The second equality in Eq. (1) relies on exact thermodynamic relations between the derivative $(\partial p/\partial \rho)_S$ and the virial coefficients of the equation of state.

Using Eq. (1), the thermodynamic temperature is deduced from measurements of the speed of sound on an isotherm that are traceable to the meter and the second. For absolute primary AGT using argon, $A_1(T)$ and $A_2(T)$ are always fitted to measurements of $u(p, T)$ and this is usually done for helium-based AGT. An acceptable alternative to fitting helium isotherms is to rely on the values of $A_1(T)$ and $A_2(T)$ calculated from quantum mechanics and statistical mechanics. [Cencek *et al.* (2012); Garberoglio *et al.* (2010)] Gavioso *et al.* (2010a) did this when they measured u^2 in helium at 410 kPa to re-determine the

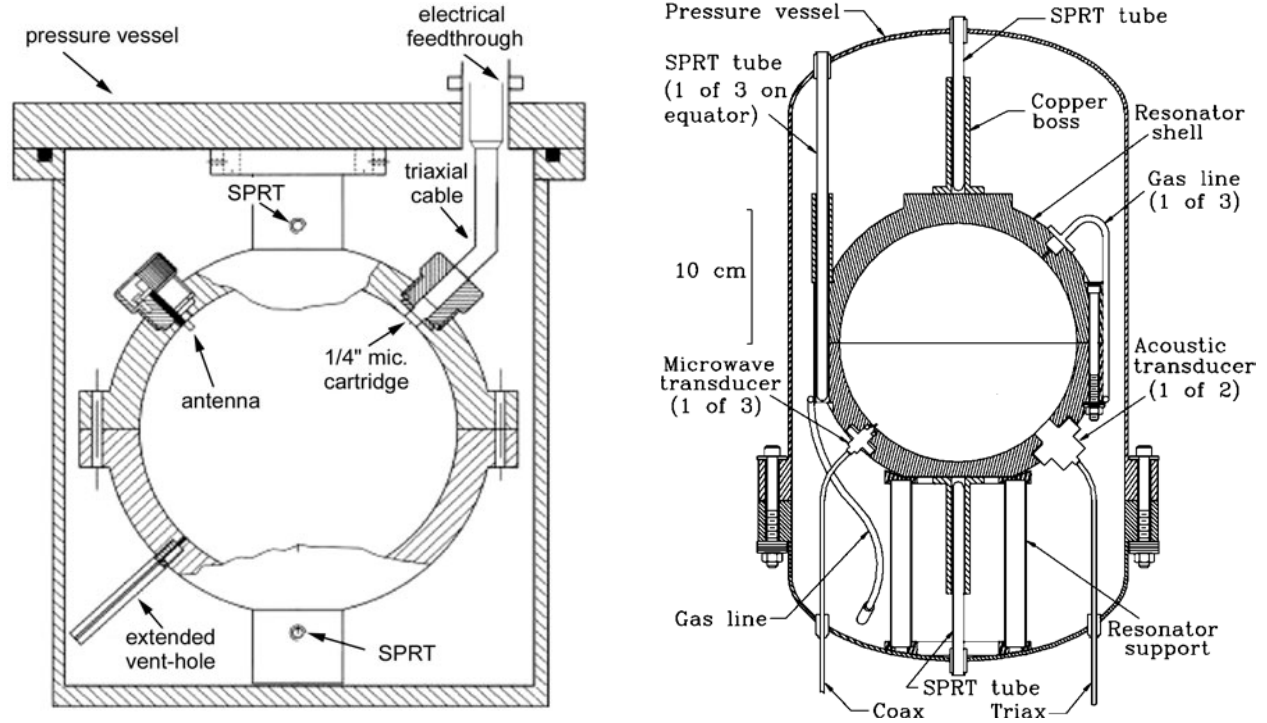


Figure 1. Two Acoustic Thermometers in their Pressure Vessels. The thermometer on the left [Benedetto *et al.* (2004)] had a cavity radius of 60 mm and it was used from 234 K to 380 K. The thermometer on the right [Strouse *et al.* (2003)] had a cavity radius of 89 mm and it was used from 273 K to 505 K. Later, two acoustic transducers were replaced with ducts and it was used up to 633 K. [Ripple *et al.* (2013)]

product $k_B T_{TPW}$ with a relative standard uncertainty of 7.5×10^{-6} . In their realization of AGT, the uncertainties of $A_1(T)$ and $A_2(T)$ contributed less than 1×10^{-6} to the relative uncertainty of $k_B T_{TPW}$. (In this Appendix, all uncertainties are standard uncertainties with coverage factor $k = 1$ corresponding to a 68 % confidence interval.) Because the calculated values of $A_1(T)$ and $A_2(T)$ for helium are functions of the *thermodynamic temperature*, they are part of the model for the realization of AGT.

Since 1979, absolute primary AGT has been conducted only near T_{TPW} and only using highly-refined cavity resonators with fixed dimensions to re-determine the product $k_B T_{TPW}$. Several groups have measured the speed of sound in argon or helium near T_{TPW} with relative uncertainties near 1×10^{-6} or less. [Moldover *et al.* (1988); Pitre *et al.* (2011); Zhang *et al.* (2011); Gavioso *et al.* (2011); de Podesta *et al.* (2011)] With one exception discussed below, these groups deduced the speed of sound from measurements of the resonance frequencies of the radially-symmetric oscillations of helium or argon contained within an approximately spherical cavity using the relationship:

$$u = \frac{f_a - \Delta f_a}{z_a} (6\pi^2 V)^{1/3} . \quad (2)$$

Here f_a is the measured resonance frequency of the gas oscillation in the mode designated by the subscript “a”, Δf_a is the sum of corrections to the unperturbed resonance frequency $f_{a,0}$ (Section 3), V is the volume of the cavity, and z_a is a mode-dependent acoustic eigenvalue that was calculated from the shape of the cavity. For the radially-symmetric acoustic modes of a nearly spherical cavity, the eigenvalues z_a are not sensitive to smooth, volume-preserving departures from a spherical shape in the first order of perturbation but are sensitive in higher orders of perturbation theory. Thus, z_a can be calculated with a fractional uncertainty on the order of $(5 \times 10^{-4})^2$ for a cavity manufactured to the readily-attainable tolerance 5×10^{-4} . [Mehl and Moldover (1986)] Then, u can be measured with an uncertainty

on the order of 10^{-6} if the frequency corrections Δf_a and the cavity's volume V are known with similar uncertainties.

The volume of nearly spherical cavities has been determined with fractional uncertainties of 1×10^{-6} or less by weighing the quantity of mercury [Moldover *et al.* (1988)] or of water [Underwood *et al.* (2012)] that just filled the cavity and relying on literature measurements of the density of these well-characterized liquids. Alternatively, microwave resonances have been used to accurately determine the volume of finely-machined, nearly-spherical, copper-walled cavities with relative uncertainties on the order of 10^{-6} using the relationship:

$$c = \frac{n \langle f_m - \Delta f_m \rangle_p}{z_m} (6\pi^2 V)^{1/3} \quad (3)$$

Here, c is the defined speed of light in vacuum, f_m is the measured microwave frequency, n is the refractive index of the gas in the cavity at the pressure p , z_m is a mode-dependent microwave eigenvalue, and $\langle f_m - \Delta f_m \rangle_p$ is the average of the corrected frequencies of the $(2l + 1)$ microwave modes that would be degenerate in a perfect spherical cavity. ($l = 1, 2, 3, \text{etc.}$) Usually, only the triply-degenerate $l = 1$ modes are used. Equation (3) exploits the theorem that the average frequency of the $(2l+1)$ modes is invariant in the first order of perturbation theory but sensitive to small, smooth departures from a spherical shape in higher orders. [Mehl and Moldover (1986)] In one remarkable example, the fractional difference between a microwave volume determination and a weighing volume determination was $(0.46 \pm 1.81) \times 10^{-6}$. [Underwood *et al.* (2012)]

The microwave measurements are simplified if the cavity has a “quasi-spherical” shape, that is, a shape that differs from spherical by just enough to separate the degenerate microwave frequencies, but not so much that the accurate calculation of the microwave and acoustic eigenvalues requires detailed measurements of the shape. [Mehl *et al.* (2004)] Typically, a quasi-spherical AGT cavity approximates a triaxial ellipsoid with axes in the ratios $1:(1+e):(1-e)$ and with $0.0005 < e < 0.001$. For this family of shapes, the electromagnetic eigenvalues z_m are known with extraordinarily small uncertainties. [Mehl (2009); Edwards and Underwood (2011)] For absolute primary AGT with the lowest possible uncertainties, quasi-hemispherical copper cavities have been manufactured by diamond turning. A pair of carefully-aligned, quasi-hemispheres bolted together creates a quasi-spherical cavity. For relative primary AGT, quasi-hemispherical cavities have been machined out of cylindrical billets of stainless-steel, aluminum, and copper using a numerically-controlled milling machine.

The most attractive features of absolute primary AGT conducted with a noble-gas-filled, quasi-spherical cavity resonator are evident when combining Eqs. (1) – (3):

$$\left[\frac{f_a - \Delta f_a}{z_a} \frac{z_m c}{n \langle f_m - \Delta f_m \rangle_p} \right]^2 = \frac{5k_B T}{3m} + A_1(T)p + A_2(T)p^2 + \dots \quad (4)$$

In the lowest order, $k_B T$ is determined by the ratio (speed of sound)/(speed of light) which is proportional to ratios of measured frequencies. The pressure and the dimensions of the cavity only appear in corrections to the lowest order.

We emphasize that Eq. (4) is always applied to measurements made with several different microwave and acoustic modes at each temperature and pressure. This redundancy facilitates very precise tests of the theories for the frequency corrections Δf_a , Δf_m and for the eigenvalues z_a and z_m . Indeed, redundancy distinguishes AGT from other forms of gas thermometry.

Because the leading term of Eq. (4) contains the ratio T/m where m is average atomic mass of the gas, the uncertainty of m contributes directly to the uncertainty of T . Commercially prepared helium is predominantly the isotope ^4He with a sub-part-per million concentration of the isotope ^3He ; therefore m is well known for chemically purified ^4He . [Mook (2000)] In contrast, commercially prepared argon has significant concentrations of several isotopes and the isotopic composition changes from bottle to bottle, even from a single supplier. Therefore, it is difficult to determine m of an argon sample with a relative

uncertainty on the order of 10^{-6} . However, it has been accomplished using isotopic argon standards and analysis for chemical impurities, including other noble gases. [Moldover *et al.*, (1988); Zhang *et al.* (2011); Valkiers *et al.* (2010); Mark *et al.* (2011)]

Quasi-spherical cavities are not essential for accurate, absolute primary AGT. Zhang *et al.* (2010, 2011) re-determined $k_B T_{TPW}$ using the non-degenerate, longitudinal acoustic modes of an argon-filled, fixed-path-length cavity. The ends of their cavity were not exactly perpendicular to the cavity's axis; however, this shape imperfection does not change the eigenvalues of the longitudinal modes in the first order of perturbation theory. Thus, a measurement of the average length of the cavity was sufficient for accurate AGT and it was accomplished using two-color optical interferometry. [Zhang *et al.* (2011)] If all the surfaces of the cavity were conducting, microwave modes could have been used for determining the average length. The non-degenerate radial modes of a cylindrical cavity could also be used for AGT if the average radius of the cylinder were determined from microwave resonances.

For completeness, we note that before 1979, absolute primary AGT was conducted using cylindrical, acoustic cavity resonators containing a moveable piston that varied the cavity's length. Measurements in the range from 1.2 K to 423 K achieved standard uncertainties of $10^{-4} T$ to $5 \times 10^{-4} T$. [Plumb and Cataland (1966); Grimsrud and Werntz (1967); Gammon (1976)] In 1979, Colclough *et al.* used a variable-length cavity at T_{TPW} and achieved the low standard uncertainty $8 \times 10^{-6} k_B T_{TPW}$. [Colclough *et al.* (1979)] During the past 30 years, the understanding of cavity resonators, together with their associated transducers and ducts that deliver and remove gas, has increased greatly. In contrast, the mechanical problems of making and using a cylindrical cavity with a movable piston have not changed. Therefore, it is unlikely that variable-length cavities will be used for AGT in the future.

1.2. Overview of Relative Primary AGT

Relative AGT determines the ratio of two (or more) thermodynamic temperatures from measurements of the ratios of speeds-of-sound conducted on the isotherms of interest. (We identify one isotherm as the reference temperature T_{ref} and a second isotherm by T .) Relative AGT uses Eq. (1) at the unknown temperature T and the reference temperature T_{ref} to form the ratio:

$$\left[\frac{u(T)}{u(T_{ref})} \right]^2 = \frac{T + m \left[A_1(T)p + A_2(T)p^2 + \dots \right] / (\gamma_0 k_B)}{T_{ref} + m \left[A_1(T_{ref})p + A_2(T_{ref})p^2 + \dots \right] / (\gamma_0 k_B)} \quad (5)$$

In contrast with absolute primary AGT, the ratio $[u(T)/u(T_{ref})]^2$ in Eq. (5) can be accurately measured without realizing either the meter or the second. The ratio measurement does require measuring ratios of lengths and times (or frequencies) with low uncertainties.

The average molecular mass m of the thermometric gas does not appear in the leading term in Eq. (5) because of the implicit assumption that m is identical at T and T_{ref} . Thus, the thermometric gas for relative AGT could be a noble gas composed of several isotopes or a noble gas with a small concentration of noble gas impurities, provided the gas mixture does not fractionate in the acoustic thermometer.

Since 1999, relative AGT has been conducted in the wide temperature range 7 K to 552 K. [Moldover *et al.* (1999); Ewing and Trusler (2000); Benedetto *et al.* (2004); Pitre *et al.* (2006); Ripple *et al.* (2007)] In the sub-range 234 K to 380 K, the results of Benedetto *et al.* (2004) overlap the results of either Moldover *et al.* (1999) or Ripple *et al.* (2007). These independently realized versions of relative AGT had very different experimental details; however, their results agreed within $3 \times 10^{-6} T$. Results from four independent realizations of AGT at the gallium and mercury points agreed within $3 \times 10^{-6} T$. [Pitre *et al.* (2006)] All of these realizations of relative AGT since 1999 used gas-filled, metal-walled, spherical or quasi-spherical cavity resonators to measure speed-of-sound ratios. In these realizations, the microwave and acoustic resonance frequencies of several cavity modes were measured near the

temperature of the triple point of water T_{TPW} and the frequencies of the same modes were measured at the other temperatures of interest T . The working equation has the form:

$$\left[\frac{(f_a - \Delta f_a)_{T,p}}{(f_a - \Delta f_a)_{T_{\text{TPW}},p}} \frac{\langle f_m - \Delta f_m \rangle_{T_{\text{TPW}},p}}{\langle f_m - \Delta f_m \rangle_{T,p}} \frac{n(T_{\text{TPW}}, p)}{n(T, p)} \right]^2 = \frac{T + \left(\frac{m}{\gamma_0 k_B} \right) [A_1(T)p + A_2(T)p^2 + \dots]}{T_{\text{TPW}} + \left(\frac{m}{\gamma_0 k_B} \right) [A_1(T_{\text{TPW}})p + A_2(T_{\text{TPW}})p^2 + \dots]} \quad (6)$$

Equation (6) exploits the fact that the ratios (acoustic frequencies)/(microwave frequencies) depend upon the cavity's volume but not upon details of the cavity' shape. Shape perturbations that might be unacceptably large for absolute primary AGT based on Eq. (4) may be acceptable for relative primary AGT because the calculated eigenvalues do not appear in Eq. (6). Indeed, the cavity plays a limited role in measuring u/c . The cavity is a temporary artifact that satisfies three conditions: (1) its dimensions are stable during the measurements of $f_a(p)$ and $\langle f_m(p) \rangle$ at the temperature T , (2) the changes of its eigenvalues between T and T_{TPW} are within the desired tolerance. (Small, smooth changes in the shape of the cavity, such as those caused by anisotropic thermal expansion [Moldover *et al.* (1999); Pitre *et al.* (2006)] affect the eigenvalues only in the second order and higher orders.), and (3) any difference between the cavity's acoustic and microwave volumes (resulting, for example, from an oxide layer) are nearly constant between T and T_{TPW} .

Equation (6) may be used with sufficient accuracy within a degree or so of T_{TPW} ; it is not necessary to set a gas thermometer to exactly T_{TPW} . We expect that some AGTs will use Eq. (6) or its equivalent with reference temperatures T_{ref} far from T_{TPW} . For example, one relative primary AGT might be used to accurately measure the thermodynamic temperature of the hydrogen point T_{H_2} and a second AGT, specifically adapted to low temperature measurements, might be referenced to T_{H_2} .

Many of the specialized, absolute primary AGTs that were developed to re-determine $k_B T_{\text{TPW}}$ used circulating liquid baths for the outermost stage of their thermostats. After comparatively minor modifications of their thermostats, these thermometers could be used for absolute primary AGT throughout a modest range of temperatures, both above and below T_{TPW} . It is unlikely that any of these instruments could function at temperatures well above T_{TPW} , where the reliability of transducers and the stability and mutual compatibility of materials drives the design of all thermometers. Instead, high-temperature acoustic thermometers will use apparatus designed for the environment and will rely on speed-of-sound ratio measurements instead of more difficult absolute measurements. [Ripple (2003)]

2. Measuring Resonance Frequencies.

2.1. Acoustic and Microwave Transducers

2.1.1. Acoustic Transducers

Accurate AGT requires a sound generator and a sound detector that perturbs the cavity's acoustic and microwave resonances in only small, predictable ways. The transducers should have a smooth frequency response; however, a flat response is not necessary. If the transducers are mounted either in or on the cavity's shell, they must not contaminate the thermometric gas and they should have a small moving mass to minimize the coupling between the transducers through motion of the shell. These criteria have been satisfied by home-made electret microphones, small, commercially-manufactured, capacitive microphones, piezoelectric (PZT) "benders", and remote transducers coupled to the cavity by ducts.

If a capacitive microphone is directly exposed to the thermometric gas, it should be assembled from ceramic and metal parts but not from polymers to minimize the chances of contaminating the gas. The moving part of the capacitor is a thin (typically, 7×10^{-6} m thick), fragile, stretched, metal, membrane with a very low mass. For generating sound, the capacitor can be driven by an alternating voltage at the frequency f , either with or without a DC bias voltage. With a DC bias, its diaphragm will oscillate at the

frequency f ; without a bias, the oscillation will be at frequency $2f$. Operation in the $2f$ manner circumvents electrical cross-talk that might occur between the large driving voltage and the small voltage generated by the detector. Capacitive microphones have been mounted with their membranes flush with the inside wall of a cavity resonator where they perturb the microwave resonance frequencies of the cavity slightly. Because of their small size and small gas-filled volume, the microphones produce only small, predictable, (and experimentally-verified) perturbations to the acoustic resonance frequencies. [Guianvarc'h *et al.* (2009)] When used as a detector, capacitive microphones require a large DC bias voltage and precautions to minimize the parasitic capacitance between the detector and a high-impedance preamplifier. (Some have used a triaxial cable with a driven guard electrode leading from the detector to a high-impedance, remote preamplifier.) At temperatures above approximately 550 K, Ripple *et al.* (2007) observed unacceptably high noise that resulted from erratic electrical leakage through ceramic cable insulators subjected to a high-voltage bias. The electrical dissipation within capacitive microphones is negligible.

In contrast with capacitive microphones, ceramic piezoelectric transducers are rugged, massive, and low-impedance electrical sources. Zhang *et al.* (2011) mounted piezoelectric transducers on the outside of cavity resonators and coupled them to the gas inside the cavity through a 0.2 mm to 0.3 mm thick diaphragm machined into the wall of the cavity. Thus, the transducers did not contact the gas inside the cavity and could not contaminate it. The comparatively thick coupling diaphragm changed neither the shape nor the electrical conductivity of the interior surface of the cavity; therefore it would not perturb the microwave resonance frequencies of the cavity if they had been measured. Piezoelectric transducers generate small predictable perturbations to the acoustic modes of the cavity. [Lin *et al.* (2010)] Piezoelectric transducers do generate heat. Zhang *et al.* did not report problems resulting from mechanical coupling of PZT transducers to the walls of the cavity.

Ripple *et al.* (2013) used a duct to conduct sound from a remote piezoelectric sound generator at ambient temperature into a cavity resonator at 600 K and a second duct to conduct sound out of the cavity to a remote commercially-manufactured sound detector at ambient temperature. This arrangement enabled AGT at high temperatures where commercially manufactured capacitive microphones and piezoelectric transducers will not function. Theory is helpful for guiding the design of such ducts and for computing the small perturbations they generate to the acoustic resonance frequencies of the cavity. [Gillis *et al.* (2009)]

Ewing and Trusler (2000) successfully used home-made electret transducers between 300 K and 90 K. Their transducers had thin polymer films in contact with the gas, which may be incompatible with maintaining gas purity at higher temperatures.

At resonance, typical acoustic pressures \wp in the cavity are in the range $0.1 \text{ Pa} < \wp < 1 \text{ Pa}$. Hamilton *et al.* (2001) predict that the perturbation of the resonance frequencies by nonlinear effects will be $(\Delta f/f)_{\text{nonlinear}} \approx [(\gamma-1)Ma/8]^2$, where $Ma \equiv |\wp|/(\rho u^2)$ is the acoustic Mach number. This condition sets an upper bound to the sound pressure for accurate AGT.

2.1.2. Coupling Microwaves to the Cavity

All the measurements of microwave frequency resonances used in AGT have used one coaxial cable to conduct the microwave fields from the generator (preferably, a network analyzer) to the cavity and another cable to conduct the fields transmitted through the cavity back to the detector (the same vector analyzer). Near the inner wall of the cavity, both cables are terminated by antennas. The simplest antenna is a short, straight extension of the inner conductor. The perturbations to the microwave frequencies produced by this kind of antenna have been modeled quantitatively and verified by measurements. [Underwood *et al.* (2010)] However, straight antennas only couple to the TM family of modes. Alternatively the cables can be terminated with a wire loop that connects the center conductor of the cable to the outer conductor of the cable. Such loops couple to all the modes of the cavity and Pitre *et al.* (2006, 2011) measured the frequency perturbations produced by the loops using a substitution method.

If no precautions are taken, the coupling wires or loops will perturb the acoustic resonance frequencies. These perturbations have been drastically reduced by recessing the wires or loops in holes in the cavity's wall and then filling the recesses with a material such as epoxy or vacuum grease which is transparent to the microwaves. If the filling material has a high acoustic impedance and terminates at the surface of the cavity, its perturbations to the acoustic frequencies will be negligible. The perturbations from imperfect terminations are discussed in detail by Pitre *et al.* (2011) in their Section 4.4.2.

2.2. Acquiring and Fitting Frequency Data

For accurate realizations of AGT, we recommend measuring the acoustic resonance frequencies and the microwave resonance frequencies at the same time, that is, while the thermometric gas is in the cavity. When this is done, the volume (and the average radius) of the cavity at the pressure under study is determined from the product $n(f_m - \Delta f_m)$ using Eq. (3) and no correction is needed for the deformation of the cavity under hydrostatic pressure. (See Section 8.1 for values of the refractive index.)

Approximate values of the acoustic resonance frequencies f_N and half-widths g_N are obtained from either preliminary measurements or a model. Then, the sound generator driven by a frequency synthesizer is stepped through discrete frequencies and the in-phase u and quadrature v signals at the detector are measured using a lock-in amplifier. (Before making a voltage measurement, it is necessary to wait at each frequency for a multiple of τ_{slow} , the slowest relaxation time needed to reach a steady state. The value τ_{slow} could be either $1/g_N$ or the post-detection time constant of the lock-in amplifier, or the settling time of the frequency tracking circuit in the lock-in amplifier.) A simple protocol uses 11 frequencies starting at $f_N - g_N$ and ending at $f_N + g_N$ with steps of $g_N/5$. Then, the frequency sweep is reversed by starting at $f_N + g_N$ and ending at $f_N - g_N$ with steps of $-g_N/5$. Alternative protocols, such as using more frequencies, taking data over a range wider than $f_N \pm g_N$, and spacing the points at selected, unequal frequency intervals, will reduce the uncertainty of the fitted parameters in many circumstances. The frequencies and complex voltages are fitted by the resonance function:

$$u + iv = \frac{ifA}{f^2 - (f_N + ig_N)^2} + B + C(f - \tilde{f}) + D(f - \tilde{f})^2 \quad (7)$$

where, A , B , C and D are complex constants; $F_N = f_N + ig_N$ is the complex resonance frequency of the mode N under study and the parameter \tilde{f} is fixed at an arbitrary value near f_N . The parameters C and D account for the effects of possible cross talk and the "tails" of the modes other than N . At high gas densities, the term $D(f - \tilde{f})^2$ may not be significant. At low densities, corrections to Eq. (7) may be needed. (Section 3.1)

For AGT, the microwave resonance frequencies are determined by sweeping through triplets of microwave resonances. Typically, data are acquired at 100 or more frequencies and they are fit to a generalization of Eq. (7) that contains a sum of three terms with resonance denominators. Then, the fitting function has 3 complex values of A , 3 values of f_N , and 3 values of g_N in addition to the background terms. For an ideal cavity, the 3 values of g_N would vary as $(f_N)^{-1/2}$; in practice, the values of g_N are larger for the modes that have currents crossing the joint between the quasi-hemispheres than for the modes with currents parallel to the joint. (For particular diamond-turned copper spheres the "joint" effect on g_N was only $\sim 2 \times 10^{-7} f_N$) Because the microwave Q s are a factor of 10 or more larger than the acoustic Q s, corrections to the microwave frequencies of order $1/Q^2$ have a negligible effect on k_B .

The frequency references for the microwave vector analyzer and the frequency synthesizer that drives the sound generator may be locked together. If this is done, errors that might arise from inaccuracies in either reference frequency cancel out of the ratios f_a/f_m which appear in Eqs. (4) and (6).

3. Theoretical Corrections to Acoustic Resonance Frequencies

Here, we discuss corrections to the raw acoustic data that are based on reliable theories. [Benedetto *et al.* (2004) has a compact list of the corrections for a spherical cavity; Zhang *et al.* (2011) has a compact list of the corrections for a cylindrical cavity.] The theory for the half-widths of the acoustic resonances requires accurate values of the viscosity and thermal conductivity of the thermometric gas. (Section 3.4) However, the theory does not contain parameters that are determined from AGT. Thus, a comparison of the theory of the half-widths obtained with a particular acoustic thermometer provides a parameter-free assessment of the understanding of that thermometer under the conditions of use.

3.1 Thermal and Viscous Boundary Layers

During each acoustic cycle, heat exchange between the gas and the shell surrounding the cavity results in a thermo-acoustic boundary layer in the gas that is characterized by an exponential decay length $\delta_T \equiv [\lambda/(\rho C_p \pi f)]^{1/2}$. Here λ is the thermal conductivity of the gas, ρ is its density, and C_p is the constant-pressure heat capacity which is exactly $5R/2$ for monatomic gases in the limit of zero density.) For the radially-symmetric acoustic modes of a spherical or quasi-spherical cavity with radius a , the boundary layer contributions to the real and the imaginary (half-width) parts of the resonance frequencies are:

$$\frac{\Delta f_{\text{therm}} + i g_{\text{therm}}}{f_{a,0}} = \left((-1+i)(\gamma-1) \frac{\delta_T}{2a} - i(\gamma-1)(4\gamma-2) \left(\frac{\delta_T}{2a} \right)^2 \right) \left[1 - \frac{(\delta_T \lambda)_{\text{shell}}}{(\delta_T \lambda)_{\text{gas}}} \right], \quad (8)$$

where $f_{a,0}$ is the unperturbed resonance frequency. Thus, Δf_{therm} and g_{therm} are equal and both increase at low density as $\rho^{-1/2}$. For typical AGT, $50 \times 10^{-6} < \Delta f_{\text{therm}}/f < 200 \times 10^{-6}$ and this is the largest correction to the raw data. The corresponding fractional corrections to $\Delta T/T$ are $100 \times 10^{-6} < \Delta T/T < 400 \times 10^{-6}$.

The term in square brackets on the right hand side of Eq. (8) accounts for the penetration of the thermal oscillations into the shell. [Moldover *et al.* (1988)] This correction will be important when AGT is conducted in copper-walled cavities below 10 K. Measurements at low densities have detected the term proportional to $(\delta_T/2a)^2$. [Gillis (2012)] Often, an equation similar to Eq. (8) is written where $f_{a,0}$ is replaced by f_a , the measured resonance frequency. In that case, the entire term proportional to $(\delta_T/2a)^2$ should be multiplied by $1/2(3\gamma-1)/(2\gamma-1) \approx 6/7$.

The term γ in Eq. (9) is the largest contributor to the half-widths of the acoustic resonances; thus, measurements of the half-widths are a critical test of the theory of the boundary layer correction. The agreement between measurement and theory is remarkable. In fact, Gillis (2012) was motivated to derive the correction of order $(\delta_T/a)^2$ by the observation that the sum $(g_{\text{therm}} + g_{\text{vol}})/f$ obtained from Eqs. (8) and (11) was greater than the measured values g_{meas}/f by $\sim 2 \times 10^{-6}$ at low densities.

In a cylindrical cavity, momentum exchange between the oscillating gas and the nearly stationary walls of the cavity results in a viscous boundary layer in the gas that is characterized by an exponential decay length $\delta_v \equiv [\eta/(\rho \pi f)]^{1/2}$, where η is the viscosity. Both the viscous boundary layer and the thermal boundary layer lead to mode-dependent perturbation to the frequencies and half-widths. For the longitudinal modes of a cylinder these are

$$\frac{\Delta f_{\text{therm}} + i g_{\text{therm}}}{f_{a,0}} + \frac{\Delta f_{\text{visc}} + i g_{\text{visc}}}{f_{a,0}} = (-1+i)(\gamma-1) \frac{\delta_T}{2a} \left(1 + \frac{2a}{L} \right) + (-1+i) \frac{\delta_v}{2a}, \quad (9)$$

where a and L are the radius and length of the cylinder, respectively. [Zhang *et al.* (2011)] Because the energy losses from momentum exchange and heat exchange add, the Q_s of the radially-symmetric modes of a spherical cavity are approximately five times larger than the Q_s of the longitudinal acoustic modes

of a cylindrical cavity if both cavities have the same length and $L \approx 2a$. For the same reason, the frequency corrections are approximately five times larger ($250 \times 10^{-6} < \Delta f_{\text{therm}}/f < 1000 \times 10^{-6}$) at the same pressures. To reduce these corrections, the optimum pressures for AGT conducted with a cylindrical cavity are probably higher than the optimum pressures for AGT conducted with a spherical cavity.

For convenience, we define the surface contribution to the Q of a cavity by $(Q_{\text{surf}})^{-1} = 2(g_{\text{therm}} + g_{\text{visc}})/f$ of a cavity. When raw acoustic data are acquired at low gas densities and fitted by the resonance function, Eq. (7), the values f_{fit} and $Q_{\text{fit}} \equiv f_{\text{fit}}/(2g_{\text{fit}})$ resulting from the fit should be corrected to account for the frequency dependence of g in the resonance formula. Gillis *et al.* (2004) deduced the formulas

$$\frac{f_{\text{corr}} - f_{\text{fit}}}{f_{\text{fit}}} \approx -\frac{1}{8} Q_{\text{surf}}^{-2} \quad \text{and} \quad Q_{\text{corr}}^{-1} - Q_{\text{fit}}^{-1} \approx -\frac{1}{4} Q_{\text{surf}}^{-2} \quad (10)$$

Smaller corrections of order $1/Q^2$ are generated by the 2nd order correction to the thermo-acoustic boundary layer, sound attenuation throughout the volume of the gas Q_{vol} [Gillis *et al.* (2004)], and by the background terms $C(f - \tilde{f})$ and $D(f - \tilde{f})^2$ in Eq. (7).

3.2 Attenuation of Sound

Under the conditions of AGT, the shift of the resonance frequency caused by the attenuation of sound throughout the volume of a resonant cavity is negligible; however, the attenuation adds a term to the half-widths of the acoustic modes given by:

$$\frac{g_{\text{vol}}}{f_a} = \left(\frac{\pi f}{u} \right)^2 \left[\frac{4}{3} \delta_v^2 + (\gamma - 1) \delta_T^2 \right] . \quad (11)$$

3.3 Smaller acoustic perturbations

The literature contains calculations of the perturbations to the complex acoustic resonance frequencies resulting from ducts that conduct gas (and sound) into and out of a cavity [Gillis *et al.* (2009); Mehl *et al.* (2004)], holes drilled through the shell (a short duct terminated by a large volume) [Moldover *et al.* (1986)], acoustic transducers [Guianvarc'h *et al.* (2009)], and slits that might surround a transducer or a cable. [Mehl *et al.* (2004)] As discussed in Section 2.1.2 above, the acoustic effects of straight and looped microwave antennas at and below ambient temperature have been circumvented rather than modeled. Perhaps this approach can be extended to high temperatures by replacing epoxy with an alternative, high-temperature material. Otherwise, models must be developed for absolute primary AGT. For relative primary AGT, the geometry of ducts, ports, antennas, and other shape perturbations should be designed so that the perturbations largely cancel when measuring ratios of thermodynamic temperature. A well-designed AGT will ensure that the difficult-to-measure narrow dimension of any slit is much smaller than δ_v so that the perturbation from the slit is small.

3.4 Thermophysical Properties of Helium and Argon

Accurate values of the density ρ , thermal conductivity λ , and viscosity η of the thermometric gas are required to correct the measured acoustic frequencies for the thermo-viscous boundary layer and sound attenuation. Accurate values of the density are needed to calculate the refractive index.

The density is calculated from the measured pressure and temperature using the virial equation of state. For helium, accurate values of the second coefficients were calculated by Cencek *et al.* (2012) and accurate values of the third virial coefficient were calculated by Garberoglio *et al.* (2010) For argon,

multi-parameter empirical equations of state have been used [Tegeler *et al.* (1999)]. However, theory-based correlations are under way and accurate *ab initio* calculations will be available within a few years.

The most accurate, zero-pressure values of the thermal conductivity and viscosity of helium were calculated *ab initio* from quantum mechanics and statistical mechanics with a fractional uncertainty on the order of 10^{-5} near ambient temperature. [Cencek *et al.* (2012)] Thus, the uncertainty of these transport properties makes a negligible contribution to the uncertainty of helium-based AGT.

In the range $200 < T/K < 400$, the most accurate values of the viscosity of argon can be obtained by combining calculated values of the viscosity of helium η_{He} [Cencek *et al.* (2012)] with the measurements by May *et al.* (2007) of the ratio $\eta_{\text{Ar}}/\eta_{\text{He}} \equiv (\text{viscosity of argon})/(\text{viscosity of helium})$. In this temperature range the fractional uncertainty of η_{Ar} is 0.00011. In the same temperature range, the most accurate values of the thermal conductivity of argon have the fractional uncertainty 0.00012; they are obtained by combining η_{Ar} with calculated values of the Prandtl number $Pr \equiv C_p \eta/\lambda$. [May *et al.* 2007] To estimate the thermal conductivity of argon above 400 K, Vogel *et al.* (2010) used an *ab initio* argon-argon interatomic potential. The resulting values of the thermal conductivity and the viscosity have estimated fractional uncertainties of 0.0005 to 0.001.

4. Theoretical Corrections to the Microwave Resonance Frequencies

4.1 Microwave Boundary Layer

The penetration of the microwave fields into the wall bounding the cavity contributes to the half-widths of the microwave resonances g_m and reduces the resonance frequencies by the same amount. For the $\text{TM}lm$ modes in a quasi-spherical cavity these perturbations are:

$$\frac{\Delta f_m + i g_m}{f_m} = (-1 + i) \frac{\delta_m}{2a} \left(1 - \frac{2}{\nu_m^2} \right)^{-1} \quad \text{with} \quad \delta_m = \frac{1}{\sqrt{\pi f_m \mu \sigma}} \quad . \quad (12)$$

In Eq. (12), δ_m is the microwave penetration length, ν_m is a microwave eigenvalue, and μ and σ are the magnetic permeability and conductivity of the shell, respectively. (For the $\text{TE}lm$ modes, the term $2/\nu_m^2$ in Eq. (12) is absent.) For a non-magnetic stainless-steel wall near ambient temperatures, Moldover *et al.* (1999) assumed that μ is identical with the permeability of free space and σ is identical to the conductivity of the bulk metal measured near zero frequency. The latter assumption fails for copper at low temperatures where σ in the thin penetration layer ($\delta_m \sim 1 \mu\text{m}$) is sensitive to impurities and strain that may remain after machining and/or polishing and to the anomalous skin effect (Section 4.3). However, the small value of δ_m implies that AGT is relatively insensitive to this assumption. [Mehl *et al.* (2004)] Instead of estimating δ_m from external measurements, one can calculate δ_m from Eq. (12) and the measured values of the half-widths g_m for those modes where the currents flow parallel to the seam where the quasi-hemispheres meet. This calculation sets a lower bound to δ_m . Measured values of g_N can exceed theoretical values of g_m because of losses associated with currents that cross the joint between the quasi-hemispheres. This extra contribution to g_m was only of order $2 \times 10^{-7} f_m$ in two diamond-turned, copper quasi-spheres, but larger in other cases.

4.2 Antennas and instruments

Underwood *et al.* (2010) made a thorough study of the small perturbations to the microwave resonance frequencies resulting from a cylindrical hole in the wall of a cavity, a junction between a coaxial cable and a cavity, and a straight antenna. If the antenna is no longer than the radius of the cable r_c or hole, all of these perturbations are on the order of $(r_c/a)^3$, which can be less than 1×10^{-6} . Furthermore,

Underwood *et al.* (2010) showed that the perturbations from the energy conducted out of a cavity by coaxial cables are even smaller.

The electrical conductivity of the membranes of the acoustic transducers may be lower than the conductivity of the wall bounding the cavity. This will reduce the microwave frequencies and increase their half-widths by equal amounts. This effect could be measured by substitution.

4.3 Anomalous Skin Effect

If AGT is conducted at low temperatures in a copper-walled cavity, the anomalous skin effect should be considered. [Podobedov (2009)] If the copper is pure enough, the microwave penetration depth at a given frequency calculated from Eq. (12) may become smaller than the mean-free-path of the conduction electrons. If so, only a small fraction of the conducting electrons spend enough time within the conducting layer to contribute to the conductivity at microwave frequencies. Then, the microwave conductivity is less than that inferred from measurements made at DC or at lower frequencies and the frequency-dependence of the penetration depth is anomalous.

5. Phenomenological Corrections to Acoustic Resonance Frequencies

The corrections discussed in Sections 3 and 4 are based on reliable theories and, except for the electrical conductivity of the cavity's walls, use parameters that are determined with sufficiently low uncertainties from the cited references that do not rely on AGT. We now consider corrections resulting from two phenomena that limit the range of the measurements used for AGT. At high densities, the limiting phenomenon is the elastic response of the resonator's walls to the acoustic oscillations. At low densities, the gas-shell interaction on the scale of the mean free path of the gas is limiting. The theories for these phenomena involve parameters that must be determined for each acoustic thermometer from measurements using that thermometer.

5.1 Elastic Recoil of the Resonator's Walls

The effects of shell motion on the gas resonances in spherical [Mehl (1985)] and cylindrical [Zhang *et al.* 2010] shells have been calculated. The theory predicts that, when a gas resonance is not too close to a shell resonance, the frequency of the gas resonance is shifted by

$$\frac{(\Delta f_l)_{\text{shell},i}}{f_l} \approx -(\rho u^2)_{\text{gas}} \frac{G_{i,l}}{1 - (f_l/f_{\text{shell},i})^2}, \quad (13)$$

where the subscript l represents the indices of a gas mode, the subscript i represents the indices of a shell mode, and $G_{i,l}$ is a compliance that depends upon the geometry of the shell, the gas mode l , and elastic properties of the resonator's walls. The perturbation $(\Delta f_l)_{\text{shell},i}$ is very nearly a linear function of the pressure on an isotherm because $(\rho u^2)_{\text{gas}}$ is nearly proportional to the pressure under conditions of AGT. Thus, a poor estimate of the compliance $G_{i,l}$ will result in values of the acoustic slopes $A_1(T)$ that differ from mode to mode and are inconsistent with the thermodynamic values of $A_1(T)$.

The radially-symmetric modes of a gas within a perfect, isotropic, spherical shell will be perturbed only by the isotropic "breathing" mode of the shell. For this case, $G_{0n,\text{breathing}} = \chi_{s,\text{int}} \equiv (3/a)(da/dp_{\text{int}})$ which is the shell's compliance to internal pressure p_{int} . This isolated "breathing-mode" approximation accurately represented the behavior of the shell used by Moldover *et al.* (1999) for acoustic thermometry from 217 K to 303 K. This claim of accuracy is supported by: (1) the measured value $f_{\text{breathing}} = 13.2$ kHz is only 3 % below the calculated value $f_{\text{breathing}} = 13.6$ kHz, (2) the agreement of the calculated acoustic slopes $A_1(T)$ with the values measured with five radial modes [after applying Eq.

(4)] over a range of temperatures, and (3) the agreement of the calculated value of the static compliance $\chi_{s,int}$ with two independent measurements of $\chi_{s,int}$. The isolated, breathing-mode approximation worked nearly as well for the much more compliant aluminum resonator studied by Moldover *et al.* (1986).

Gavioso *et al.* (2010b) measured the frequency perturbations $(\Delta f)_{shell,i}$ caused by the recoil of the steel shell of a spherical cavity and of the copper shell of a quasi-spherical cavity. For the steel resonator, $(\Delta f)_{shell,i}$ had at least 4 wide peaks in the range 75 % to 100 % of the predicted $f_{breathing}$. For the copper resonator, $(\Delta f)_{shell,i}$ had 3 narrow peaks centered at 85 % of the predicted $f_{breathing}$. Thus, the isolated breathing-mode approximation was a poor description of these two resonators. Finite-element models of shells show that small departures from perfect radial symmetry (such as flanges at the equatorial joint between hemispheres or small bosses at the closed end of each hemisphere) lead to only small changes in $f_{breathing}$ and only weak couplings between the radially symmetric acoustic modes and non-radial modes of the shell.

The three shells mentioned above were assembled by bolting hemispheres together. The breathing-mode model worked well for the only one of the three that had a thin, highly-compressed layer of wax sealing the hemispheres together. [Moldover *et al.* (1999)] Perhaps the poor agreement between the model and the data for the other shells resulted from the model's neglect of the joint where the hemispheres meet. For all three shells, the measured half-widths of the radial modes exceed the calculated half-widths by a constant times the pressure: $\Delta g_N = g_{N,meas} - g_{N,calc} = A_N p$. There are no accurate predictions for A_N . However, Δg_N does approach zero with decreasing pressure; therefore, the elastic recoil contributions to A_N are unlikely to cause errors in AGT.

Zhang *et al.* (2010, 2011) modeled several elastic modes of an ideal cylindrical shell that could be excited by longitudinal gas modes. These included longitudinal stretching, bending of the endplates, and center-of-mass motion. (They also modeled radial stretching.) The values of $A_1(T)$ that they measured for several longitudinal modes were inconsistent with the thermodynamic value of $A_1(T)$ after correcting for the calculated elastic recoil.

In summary, the elastic recoil of a cavity's shell cannot be predicted reliably from first principles, although a simple model has worked well in one case. In all cases, the inconsistencies among the acoustic modes approach zero linearly with decreasing pressure. We take these inconsistencies as a measure of the uncertainty of the temperature arising from the elastic recoil of the cavity's walls. An independent measure of the uncertainty of the temperature is the spread among the values of Δg_N , although this spread can arise from phenomena other than the recoil of the cavity's walls.

Acoustic thermometers operating at high temperatures will encounter larger values of the perturbations $(\Delta f)_{shell,i}$ because they will operate at higher pressures. (Section 6) Thus, they should be designed to reduce the compliances $G_{i,l}$ by making the cavity's walls of a stiff material, making the joints as stiff as possible, and making the cavity's wall as thick as practical. Several spherical acoustic thermometers have operated with the ratio (cavity radius)/(wall thickness) ≈ 5 . If the ratio had been 2.5, the elastic corrections would have been half as large.

When a gas mode and a shell mode have nearly identical frequencies, they couple strongly and the frequencies are very sensitive to the shell's properties. The frequencies exhibit an "avoided crossing" and Eq. (4) is no longer applicable. Acoustic thermometry should not be conducted in this regime. Near-crossings can be identified easily by analyzing the data from multiple acoustic modes at the same temperature and pressure.

5.2 Effects of Non-zero Mean Free Path

Ewing *et al.* (1986) discussed the acoustic consequences of the kinetic theory prediction that a temperature jump occurs at a gas-solid interface when heat is transferred across the interface. They concluded that the temperature jump increases the resonance frequencies and leaves the half-widths unchanged. For a monatomic gas, the frequency increase is

$$\frac{\Delta f_i}{f_i} = \frac{(\gamma-1)l_a}{a} \quad \text{with} \quad l_a = \left(\frac{\lambda}{p}\right) \sqrt{\frac{\pi m T}{2k_B}} \frac{(2-h)}{2h}, \quad (14)$$

where l_a is the thermal accommodation length. In Eq. (14), λ is the thermal conductivity, m is the mass of an atom, and h is the thermal accommodation coefficient. (If $h = 1$, l_a equals 1.8 times the mean free path. For argon at T_{TPW} , 100 kPa, and $h = 1$, $l_a = 118$ nm.) The coefficient h accounts for the fraction of the gas molecules incident on the solid that are reflected or re-emitted from the solid with the kinetic energy expected from the solid's temperature. Thus h might depend upon the gas, the temperature, and the microscopic conditions of the surface (such as oxidation or the presence of an oil film). The temperature jump adds the term $A_{-1}p^{-1}$ to the polynomial expansion Eq. (1). Ewing *et al.* included this term in a fit to their measurements using an argon-filled, aluminum-walled cavity and found $h = (0.84 \pm 0.05)$. For an argon-filled, steel-walled cavity, Moldover *et al.* (1988) found $h = (0.93 \pm 0.07)$ at T_{TPW} . Ripple *et al.* (2007) found the average value $h = (1.02 \pm 0.15)$ over the temperature range $271 < T/K < 552$, with no obvious temperature dependence. Benedetto *et al.* (2004) and Pitre *et al.* (2006) assumed that $h = 1$ over wide temperature ranges. Gavioso (2011) determined $h = 0.378 \pm 0.010$ for the thermal accommodation coefficient of helium on a diamond-turned copper-walled cavity. Using this experience as a guide, Moldover (2011) assumed that the uncertainty of h was 0.05 and used this value to estimate a value of the gas density below which acoustic measurements would not reduce the uncertainty of the thermodynamic temperature at T_{TPW} . (See Section 6.) In contrast with these observations, Song and Yovanovich (1987) reported values of h ranging from 0.4 to 0.1 for helium interacting with "engineering surfaces" over the temperature range 273 K to 1250 K.

The velocity of a gas oscillating in longitudinal acoustic modes of a cylindrical cavity is transverse to the solid wall bounding the cavity. In this situation, the same kinetic theory considerations which predict a temperature jump at the gas-solid interface also predict a momentum jump. [Trusler, (1991)] The momentum jump increases the resonance frequencies and leaves the half-widths unchanged. During the calibration of many spinning-rotor vacuum gauges, accurate values of the momentum accommodation coefficient were measured. In many cases the results were unequal to 1, but within a few percent of 1. [Chang and Abbott (2007)]

6. Optimizing the Range of Data Acquisition

For a given cavity resonator, there is a range of molar gas densities ρ/M that is most useful for conducting low-uncertainty AGT. (M is the average molar mass of the gas.) Moldover (2009) estimated this range for a quasi-spherical, steel-walled cavity with an inside radius of 5 cm and an outside radius of 8 cm. When filled with argon, the optimum range is $40 \text{ mol}\cdot\text{m}^{-3} < \rho/M < 200 \text{ mol}\cdot\text{m}^{-3}$ (corresponding to the pressure range $100 < p/\text{kPa} < 500$ at T_{TPW}). When filled with helium, the optimum range is $130 \text{ mol}\cdot\text{m}^{-3} < \rho/M < 400 \text{ mol}\cdot\text{m}^{-3}$ (corresponding to the pressure range $300 < p/\text{kPa} < 900$ at T_{TPW}). Although these estimates are very approximate, we will use them to discuss aspects of AGT.

Below the optimum density, the Q s of the acoustic modes decrease approximately as $p^{-1/2}$ and the signal-to-noise ratio of the frequency measurements decreases as p^{-2} , assuming the sound generator produces an acoustic pressure that is proportional to the static pressure. Also, as the density decreases, the mean free path grows as ρ^{-1} . Therefore, as the density is lowered, the uncertainty of the measured acoustic frequencies grows rapidly and the measured frequencies become increasingly sensitive to the parameter A_{-1} (Section 5.2). As the density is increased above the optimum range, the measured acoustic resonance frequencies become increasingly sensitive to the recoil of the cavity's wall (Section 5.1) and to the pressure-coefficients $A_3(T)$ and $A_4(T)$ that must be added to Eqs. (1) and (2). Thus, at higher than optimum density, one learns more about the complicated vibrations of the walls and supports of the cavity and more about the higher virial coefficients of the gas; however, this information has only a small effect on the uncertainty of the thermodynamic temperature.

The lower bound to the optimum density is, like the mean free path, approximately independent of the temperature, provided that the sensitivity of the detector of the acoustic pressure (at the wall of the cavity resonator) can be increased as T^{-1} . The upper density bound decreases with temperature because the magnitude of $A_3(T)$, $A_4(T)$, etc. increase at low temperatures.

At temperatures above approximately 90 K, both helium and argon can be used for AGT. When compared at the same temperature and pressure, argon has three advantages: (1) the corrections from $A_{-1}(T)$ are larger in helium than argon because the mean free path in helium is 1.5 times longer than in argon. (2) the Q s of the acoustic resonances are 1.7 times larger in argon than in helium leading to better signal-to-noise ratios, and (3), the speed of sound in argon is less sensitive to common impurities (Section 9). However, acoustic measurements made near the liquid-vapor coexistence curve of argon may be subject to bias from pre-condensation. [Mehl and Moldover, (1982)]

For argon in the range of optimum densities mentioned above, δ_T increases only 19 % as the temperature is increased from 273 K to 1200 K and the Prandtl number changes less than 1 %. Thus, it is possible to conduct AGT in a temperature-independent range of δ_T and δ_v simultaneously instead of a temperature-independent range of molar densities. (A temperature-independent range of δ_T and δ_v is approximately equivalent to a temperature-independent range of Q .) This alternative is advantageous because difficult-to-model acoustic perturbations that depend upon δ_T and δ_v cancel out of the ratio Eq. (6). For example, a coupling loop that extends from the end of a coaxial cable into (or nearly into) a cavity resonator will generate acoustic perturbations that are difficult to model because they depend upon the ratios of δ_l and δ_v to many lengths. A high-temperature coaxial cable will generate difficult-to-model perturbations if insulation between the center conductor and the sheath is not sealed at the cavity's wall. This would occur if, for example, the insulator were quartz tubes or sapphire beads. To the extent that differential thermal expansion can be ignored, such complex perturbations will be temperature-independent for measurements conducted at constant values of δ_l and δ_v .

7. Uncertainties from Pressure Measurements

In the AGT working equations [(3) and (6)], the pressure is used in 4 ways: 1), explicitly in calculating or fitting the terms $A_1p + A_2p^2$ that represent the pressure-dependence of u^2 , 2), implicitly, when calculating the density-dependent corrections to the acoustic frequencies such as Δf_{therm} , 3), implicitly, when calculating the refractive index n , and implicitly when fitting the thermal accommodation coefficient h in Eq. (14). Here, we consider how accurately the pressure must be measured so that each of these uses contributes no more than 10^{-6} to the fractional uncertainty of T .

If $T > 8$ K, u^2 in helium varies by less than 1 % in the density range recommended in Section 6. ($130 \text{ mol}\cdot\text{m}^{-3} < \rho/M < 400 \text{ mol}\cdot\text{m}^{-3}$) If $T > 170$ K, u^2 in argon varies by less than 1 % in the density range recommend in Section 6. ($40 \text{ mol}\cdot\text{m}^{-3} < \rho/M < 200 \text{ mol}\cdot\text{m}^{-3}$) For these "high" temperatures, a relative pressure uncertainty of 10^{-4} at p_{max} is adequate for determining $u^2(p, T)$, and therefore T with a relative uncertainty on the order of 10^{-6} . (Here p_{max} is the maximum pressure on the isotherm of interest.) If a relative pressure uncertainty of $2 \times 10^{-5} p_{\text{max}}$ is achieved, the low-temperature bounds become $T > 3$ K in helium and $T > 91$ K in argon. If A_1 and A_2 are fitted on each isotherm and their values are not checked against theoretical values, the required pressure uncertainty can be reduced to a required pressure linearity and an accurate pressure zero.

As the pressure is reduced towards the minimum pressure on each isotherm p_{min} , the fractional correction to the thermodynamic temperature from the thermo-acoustic boundary layer $(2\Delta f_{\text{therm}})/f_a$ increases as $p^{-1/2}$ and reaches, approximately, 4×10^{-4} at p_{min} for the (0,2) radial acoustic mode. If the fractional uncertainty of p_{min} is 2.5×10^{-3} , its contribution to the fractional uncertainty of T will be 1×10^{-6} .

The refractive index is calculated from the density using the Lorentz-Lorenz relation:

$$\frac{n^2 - 1}{n^2 + 2} = (A_\epsilon + A_\mu) \rho (1 + b_\epsilon(T) \rho + \dots) \quad (15)$$

The density is usually calculated from the measured temperature and pressure and an equation of state from the literature. At the maximum densities mentioned in Section 6 ($400 \text{ mol}\cdot\text{m}^{-3}$ for helium and $200 \text{ mol}\cdot\text{m}^{-3}$ for argon), $n_{\text{argon}}^2 = 1.0025$ and $n_{\text{helium}}^2 = 1.00062$. If these values of n^2 are measured with an uncertainty of approximately 10^{-6} , they will contribute a fractional uncertainty of approximately 10^{-6} to the fractional uncertainty of T . The pressure is nearly proportional to $n^2 - 1$; therefore, the required pressure uncertainties are, fractionally, 1.6×10^{-3} for helium and 4×10^{-4} for argon. At the densities used for AGT, the uncertainty of T from the uncertainty of the equation of state is negligible, except for argon at low temperatures

On each isotherm, the thermal accommodation coefficient h , or equivalently, the thermal accommodation length l_a must be fitted, together with T , A_1 , and A_2 . We estimate the mean-free-path correction to the acoustic frequencies $\Delta f_i/f_i = (\gamma - 1)l_a/a$ by assuming $h = 1$ and $a = 50 \text{ mm}$. As the argon pressure is decreased in the range recommended in Section 6, this estimate increases as p^{-1} from 0.5×10^{-6} to 2.4×10^{-6} and the corresponding correction to T increases, fractionally, from 1×10^{-6} to 4.8×10^{-6} . This p^{-1} term is easily distinguished from the $p^0 \propto T$ term, provided that the pressure measurements are a linear function of the true pressure and the zero of the pressure transducer is accurate to within a few percent of p_{min} .

The pressure uncertainties required for all 4 uses of the pressure are easily attained except when conducting AGT in helium at very low temperatures and (correspondingly low pressures) where the uncertainty of the thermo-molecular pressure gradient contributes to the pressure uncertainty.

As discussed in Section 9 below, it may be advantageous to conduct AGT while gas flows continuously from a manifold through narrow ducts to and from the cavity. If this is done, a separate duct leading from the cavity to the pressure-measurement system is desirable to make accurate pressure measurements without accounting for flow-generated pressure drops.

8. The Refractive Index and the Density

In Section 8.1, we recommend refractive index data for determining the radius of a gas-filled cavity from microwave frequency measurements. In Section 8.2, we suggest that replacing the pressure in Eqs. (4) and (6) with the density, as determined from microwave frequency measurements, might be useful for low-temperature AGT.

8.1 Data for the refractive index

For helium, the leading terms A_ϵ and A_μ in Eq. (15) are independent of the temperature and are accurately known from theory. (See Table 1.) Rizzo *et al.* (2002) calculated $b_\epsilon(T)$ using a fully quantum statistical approach. Their tabulated values vary from $-0.0031 \text{ cm}^3\cdot\text{mol}^{-1}$ at 3.8 K to $-0.126 \text{ cm}^3\cdot\text{mol}^{-1}$ at 408 K. [See Cencek *et al.* (2011) for classical values of $b_\epsilon(T)$ and their uncertainty between 77 K and 322 K.]

Table 1. Constants for estimating the refractive index from the density

Property $\text{cm}^3\cdot\text{mol}^{-1}$	Helium	Helium Reference	Argon	Argon Reference
A_ϵ	0.517 254 19(10)	Lach <i>et al.</i> (2004)	4.142 03(19)	Schmidt and Moldover (2003)
A_μ	-0.000 007 91(01)	Bruch and Weinhold (2000)	-0.000 080 9(6) ^a	Barter <i>et al.</i> (1960)
$b_\epsilon(298 \text{ K})$	-0.1035	Rizzo <i>et al.</i> (2011)	0.36	Rizzo <i>et al.</i> (2002)

^aAverage of three measurements from the literature

The value of A_ε for argon in Table 1 was measured by Schmidt and Moldover in an apparatus that had been calibrated using the theoretical values $\varepsilon(p,T)$ of helium. Because the apparatus was calibrated and used at the same pressures and temperatures (near 0 °C and 30 °C), the imperfections of the pressure measurements and the thermometry had a small effect on the uncertainty of A_ε . For argon, Rizzo *et al.* (2002) calculated $b_\varepsilon(T)$; it varies from 0.52 cm³•mol⁻¹ at 100 K to 0.31 cm³•mol⁻¹ at 408 K.

8.2 Relating the microwave frequencies to the density

The measured frequencies of a microwave multiplet are related to the refractive index by

$$n^2 = \left[\frac{\langle f_m - \Delta f_m \rangle_{\text{vac}}}{\langle f_m - \Delta f_m \rangle_p} \right]^2 \left(1 + \frac{p}{3B_T} \right)^2 \approx \left[\frac{\langle f_m - \Delta f_m \rangle_p}{\langle f_m - \Delta f_m \rangle_{\text{vac}}} \right]^2 \left(1 + \frac{\rho RT}{3B_T} \right)^2 \approx (1 + 3A_\varepsilon \rho) . \quad (16)$$

In Eq. (16), R is the universal gas constant and the subscripts ‘‘p’’ and ‘‘vac’’ denote measurements made at the pressure p and under vacuum, respectively. Also, $B_T \equiv -V/(\partial p/\partial V)_T$ is the isothermal bulk modulus of the cavity and it accounts for the shrinkage of the cavity’s volume under the hydrostatic pressure of the gas. Because the volume of the cavity is defined by an assembly of metal parts, the value of B_T of the cavity is assumed to be identical to B_T of the cavity’s wall. A typical value for copper and some steels is $B_T \approx 1.4 \times 10^{11}$ Pa near T_{TPW} .

In Eq. (16), the second approximate equality is obtained from Eq. (15) by making the approximations $(n^2 + 2) \approx 3$, $A_\mu \approx 0$ and $b_\varepsilon \approx 0$. This equality shows that the gas density is determined by A_ε and the ratio of measured frequencies, corrected by the fraction $F \equiv 2RT/(9A_\varepsilon B_T)$. We estimate $F_{\text{He}} \approx 0.007$ and $F_{\text{Ar}} \approx 0.00087$ near T_{TPW} . To deduce the density of helium with a fractional uncertainty of 10^{-4} near T_{TPW} , the relative uncertainty of F_{He} must be less than $10^{-4} / F_{\text{He}} \approx 0.014$. It might be difficult to know B_T with this low uncertainty for a cavity assembled out of copper parts. At a lower temperature, for example, 30 K, the required relative uncertainty of F_{He} (and B_T) is 0.17, an easily attained value. Thus, it is feasible to conduct helium-based AGT below 30 K by replacing the pressure in Eqs. (3) and (6) with the density deduced from Eqs. (15) and (16). Because $F_{\text{Ar}} = 8.007 \times F_{\text{He}}$, argon-based AGT using the density is feasible at and below ambient temperature.

Equation (16) requires an accurate value of $\langle f_m - \Delta f_m \rangle_{\text{vac}}$ at each temperature. Measuring $\langle f_m - \Delta f_m \rangle_{\text{vac}}$ may be time consuming because evacuating a cavity through a small duct is slow.

9. Chemical Impurities and Gas Handling

A careful accounting for impurities in the thermometric gas is essential for accurate AGT. The normalized derivative $D \equiv (1/u^2)(du^2/dx)$ of the square of speed of sound u^2 with respect to the mole fraction x of an impurity measures the influence of impurities on AGT. See Table 2.

Except for hydrogen, $|D|$ is at least 8 times larger for helium than for argon. Argon’s reduced sensitivity to impurities is one reason that argon is preferred to helium for AGT near ambient temperature. For argon, the values of D are of order 1; therefore, the mole fractions of common impurities must be near or below 10^{-6} to realize absolute AGT with uncertainties on the order of 10^{-6} . For relative AGT, any changes in the mole fractions of common impurities between T and T_{ref} must be consistent with the desired uncertainty. At high temperatures, hydrogen from outgassing is the most common impurity and must receive special attention. (See below.)

Highly-purified, commercially-supplied gas is the starting point for conducting accurate, relative AGT. The manifold that transports the gas from the supplier’s cylinder to the cavity and regulates the gas’ flow and pressure should be constructed using high-vacuum techniques. These include using tubing and fittings with electro-polished interiors and all-metal, bakeable components, (including meters and

Table 2. Sensitivity of u^2 to impurities. [Moldover et al (1988)]

Impurity	M gm/mol	γ_0	D^a in He	D^a in Ar
H ₂	2	1.4 ^a	0.23	0.68
He	4	5/3		0.9
H ₂ O	18	1.32 ^a	-3.93	0.12
Ne	20	5/3	-4.0	0.5
N ₂	28	1.4 ^a	-6.27	0.03
O ₂	32	1.4 ^a	-7.3	-0.07
Ar	40	5/3	-9.0	
CO ₂	44	1.4 ^a	-10.3	-0.37
Kr	84	5/3	-20.0	-1.1
Xe	131	5/3	-31.8	-2.3

^aValues at 273 K. For polyatomic gases, D and γ_0 are temperature-dependent.

regulators). Virtual leaks must be minimized and joints should be welded or compression-sealed with metal gaskets. The manifold should include a heated, reactive metal (getter) to remove chemically reactive impurities from the supplier's gas. These precautions should reduce the problem caused by outgassing of water from the ambient-temperature parts of the manifold noted by de Podesta *et al.* (2011).

When a well-designed manifold supplies pure gas to an acoustic thermometer, the outgassing of an impurity within the thermometer itself can contaminate the gas. Ripple *et al.* (2003) reported outgassing of hydrogen, probably from the stainless steel resonator itself. They used a residual gas analyzer to quantify the rate of hydrogen outgassing and reduced the outgassing by baking the apparatus for weeks. Such contamination can be detected and accounted for by monitoring an acoustic resonance frequency while the thermometric gas continuously flows through the cavity. If the outgassing rate is independent of the presence of the flowing gas, there will be a range of flows such that the frequency is a linear function of the flow rate with a coefficient that varies inversely as the pressure. In this situation, the measured frequency can be extrapolated to zero flow. Alternatively, one can stop the flow and measure the rate of frequency changes $df/dtime$ from which an outgassing rate can be determined. Then, all the measurements can be corrected using that outgassing rate.

Several phenomena should be considered when designing a flow system. Purge paths should be designed so that any outgassing sources (e.g., commercial transducers, mass flow controllers) are downstream of the cavity. Heat exchange between the incoming gas and the thermostat must be sufficient to prevent flow-induced thermal gradients forming in the cavity's walls. Except at very low flow rates, gas entering the cavity from a duct will flow in a jet across the cavity, "splash" off the wall opposite the entrance, and then mix with the gas already in the cavity. [Pitre *et al.* (2011)] To achieve good mixing, the outlet duct should not be opposite the entrance duct

The jet entering the cavity will dissipate its kinetic energy as it mixes with the gas already in the cavity. If the diameter of the inlet duct is too small, the kinetic energy in the jet may be large enough to generate temperature gradients within the gas inside the cavity. This phenomenon may have been observed by Pitre *et al.* (2011). Flow-generated fluctuations of the pressure in the cavity will generate corresponding temperature fluctuations in the gas on time scales of milliseconds to many seconds. The temperature fluctuations will modulate the acoustic resonance frequencies and can easily be mistaken for excess electronic noise during frequency measurements. To eliminate this phenomenon, Ripple *et al.* (2003) devised a simple, non-contaminating, rapidly-responding flow regulator.

During AGT, noble gas impurities in helium or argon are unlikely to be detected by flow-dependent frequency shifts. For example, a duct transporting helium from ambient temperature to a cold cavity can act as a cold trap that collects the argon impurity over a wide range of flow rates. Then, the composition of the helium in the cavity would be independent of flow, but dependent on the duct's and cavity's temperature causing an error in the AGT that depended on the mole fractions of the impurities.

The error could be detected by comparing the speed of sound in the helium before and after it passed through the cryostat. Argon and neon in the supplied helium gas can be detected by using sensitive gas chromatography to compare the sample gas with gravimetrically-prepared standards. A liquid-helium-cooled trap will remove argon impurities from helium.

10. Linking the Thermodynamic Temperature to T_{90}

The acoustic thermometers described above cannot be inserted into fixed-point cells, cryostats, or ovens to measure the temperature of these environments. Instead, all these AGTs have design features that facilitate linking the average thermodynamic temperature of the gas in the AGT's cavity to the ITS-90. At near-ambient and at cryogenic temperatures, the linkage has been made by installing several, redundant capsule-type rhodium-iron thermometers or capsule-type standard platinum resistance thermometers (SPRTs) in the shell surrounding the cavity. At higher temperatures, frequently-calibrated, long-stemmed SPRTs must be used to realize the ITS-90 with small uncertainties. Therefore, high-temperature acoustic thermometers should contain thermally-anchored thermometer wells to facilitate satisfactory immersion of long-stemmed thermometers and their frequent removal for recalibration. [Ripple *et al.* (2003)]

If the temperature of the shell surrounding the cavity is not uniform, the average gas temperature may differ from the temperature(s) indicated by the SPRTs. The use of multiple SPRTs may detect temperature non-uniformities such as a vertical gradient resulting from imperfections of the thermostat. To estimate the effect of a temperature drift rate ($dT/dtime$), it is convenient to define two time constants: (1) τ_{shell} which is the relaxation time for decay of thermal gradients in the shell, and (2) τ_{gas} which is the relaxation time for gas injected into the cavity to come to equilibrium with the shell. The drift generates a temperature gradient in the shell on the order of $(dT/dtime)\tau_{shell}$ and a temperature gradient in the gas on the order of $(dT/dtime)\tau_{gas}$. If a gas flows into the cavity with the volume rate V' and with the temperature difference ΔT from the cavity's temperature, the flow may generate a temperature non-uniformity as large as $\Delta T V' \tau_{gas}/V$, where V is the volume of the cavity.

11. Expected Uncertainties in AGT

Acoustic thermometers provide redundant data that are used to test the raw data and the corrections that are applied to the raw acoustic data. Routinely, the resonance frequencies and the resonance half-widths of several acoustic and several microwave modes are measured at each temperature and pressure. The frequencies of the several modes are tested for mutual consistency and the values of the half-widths are tested by comparisons with theory. This redundancy can detect many Type B uncertainties.

Up to this point, we discussed single isotherms and pairs of isotherms. In fact, the parameters that are fitted on each isotherm (A_1 , A_2 , A_{-1} , and T) discussed in Sections 1 and 5.2 account for physical phenomena that are smooth functions of the thermodynamic temperature T . All 4 parameters are also smooth functions of T_{90} , except for the discontinuity in the derivative $d(T - T_{90})/dT$ at T_{TPW} . Therefore uncertainties can be reduced and errors can be detected if the data on many, closely-spaced isotherms are simultaneously fitted by physically-motivated functions of T_{90} that have fewer parameters. For example, Moldover *et al.* (1999) fitted 6 isotherms in the temperature range $217 \text{ K} \leq T \leq 303 \text{ K}$ independently with 24 parameters and then fitted the same data with a surfaces that had either 11 or 12 parameters. With fewer parameters, the uncertainties of $T - T_{90}$ decreased. Smooth, physically-based functions with few parameters can be generated by adding a simple analytic function (such as a polynomial function of $\log(T/K)$) to a theoretically-based function (such as the second acoustic coefficient generated by Vogel *et. al* (2010) using an ab initio argon-argon potential).

Table 3 is adapted from Table 9 of Pitre *et al.* and Table 2 of Ripple *et al.* to display the most important uncertainty components in these realizations of AGT. The tabulated values are the $k = 1$ components and their quadrature sum, expressed in parts per million of T .

EDITION 2013

Table 3. Contributions to the $k = 1$ relative uncertainty of $10^6 \times (T - T_{90})/T$, determined by AGT, as implemented by Ripple *et al.* (2007) and Pitre *et al.* (2006).

T / K	Microwave measurements ^a	Thermostat and ITS-90 thermometry ^b	Acoustic measurements ^c	Gas purity	Gas properties ^d	Root sum of squares
Argon [Ripple <i>et al.</i> (2007)]						
552	1.7	0.8	3.1	0.7	0.5	3.8
550	1.7	0.8	3.0	0.7	0.5	3.6
470	1.3	1.1	1.6	0.4	0.4	2.3
466	1.3	1.1	1.4	0.4	0.4	2.4
394	1.2	0.9	1.3	0.5	0.3	2.0
367	1.1	1.0	1.1	0.5	0.3	1.9
364	1.1	1.0	1.1	0.5	0.3	1.9
333	1.0	1.1	0.8	0.0	0.3	1.8
Helium [Pitre <i>et al.</i> (2006)]						
234.31	0.9	0.6	1.3	1.5	0.0	2.2
192.08	0.8	0.8	2.1	1.5	0.0	2.9
161.39	0.9	1.1	1.9	1.5	0.0	2.7
127.55	0.9	1.4	6.0	1.5	0.0	6.4
96.41	1.1	1.2	1.5	1.5	0.0	2.7
83.801	1.2	1.1	6.4	1.4	0.0	6.8
77.857	0.9	1.2	3.6	1.4	0.0	4.1
77.657	0.9	1.2	2.2	1.4	0.0	3.0
24.551	3.7	7.7	2.0	1.4	7.7	11.8
19.679	2.5	8.1	4.1	1.4	9.6	13.7
13.837	4.3	10.1	2.9	1.4	10.1	15.2
10.293	5.8	11.7	1.0	1.4	7.7	15.5
7.0055	4.3	14.3	5.7	1.4	0.0	15.7

^aIncludes effects of: inconsistencies among modes, skin depth, antennas and transducers, and, only for argon, imperfect resolution of microwave triplets.

^bIncludes determination of T_{90} and temperature gradients

^cIncludes inconsistencies among modes and uncertainty of thermal accommodation coefficient h

^dthermal conductivity of argon and 3rd acoustic virial coefficient of helium

Table 3 summarizes two realizations of AGT; each was the first to reach the listed highest or the lowest temperature. From the experience of these pioneering measurements, lower uncertainties may be possible in the future. For example, the helium used by Pitre *et al.* might have contained either 2.5 ppm of neon or 1.1 ppm of argon (or some combination of neon and argon) that led to uncertainty contributions listed under “Gas purity”. In future work, this contribution could be reduced by improved gas analysis and/or purification. In the work of Ripple *et al.*, the uncertainty contributions listed under “Microwave measurements” might be reduced by using a quasi-spherical cavity instead of a spherical cavity with incompletely resolved microwave triplets.

The uncertainties from “Acoustic measurements” in Table 3 resulted from inconsistencies in the values of $T - T_{90}$ obtained with different acoustic modes. At many temperatures, only a few acoustic modes could be used to determine $(T - T_{90})$ because the frequencies of the gas modes and shell modes were close together. This explains the somewhat surprising difference in the uncertainty of the 77.857 K and 77.657 K isotherms in Table 3. In future thermometers, this uncertainty component might be reduced by increasing the ratio (shell thickness)/(cavity radius). At the lowest temperatures listed in Table 3, the largest uncertainty contribution comes from the realization of T_{90} . In this range AGT is more accurate than realizations of the internationally accepted temperature scale.

EDITION 2013

References

- Barter, C., Meisenheimer, R. G., and Stevenson, D. P., 1960. Diamagnetic susceptibilities of simple hydrocarbons and volatile hydrides, *J. Phys. Chem.* **64**, 1312.
- Benedetto, G., Gavioso, R. M., Spagnolo, R., Marcarino P., and Merlone A., 2004, Acoustic measurements of the thermodynamic temperature between the triple point of mercury and 380 K, *Metrologia* **41**, 74-98.
- Bruch, L. W., and Weinhold, F., 2000, Diamagnetism of helium, *J. Chem Phys.* **113**, 8667-8670. The best theoretical estimate is the Pekeris value from the first row of Table 1 plus the difference of rows 2 and 3 which is the relativistic effect.
- Cencek, W., Komasa, J., and Szalewicz, K. 2011 Collision-induced dipole polarizability of helium dimer from explicitly correlated calculations, *J. Chem. Phys.* **135**, 014301.
- de Podesta, M., Sutton, G., Underwood, R., Bell, S., Stevens, M., Byrne, T., and Josephs-Franks, P., 2011 Outgassing of water vapour, and its significance in experiments to determine the Boltzmann constant, *Metrologia* **48** L1-L6.
- de Podesta, M., Sutton, G., Underwood, R., Perkin, M., Davidson, S., and Morantz, P., 2011, Assessment of Uncertainty in the Determination of the Boltzmann Constant by an Acoustic Technique, *Intl. J. Thermophysics*, **32** 413-426.
- de Podesta, M., Underwood, R., Sutton, G., Morantz, P., Harris, P., 2012, Internal Consistency in the Determination of the Boltzmann Constant using a Quasispherical Resonator *Proc. 9th Intl. Temperature Symposium, March 19-23, 2012, Anaheim, CA, American Institute of Physics*, (In press).
- Chang, R. P., and Abbott, P. J., 2007, Factors affecting the reproducibility of the accommodation coefficient of the spinning rotor gauge, *J. Vac. Sci. Technol.* **A25**, 1567-1576.
- Cencek, W., Przybytek, M., Komasa, J., Mehl, J.B., Jeziorski, B., and Szalewicz, K., 2012, Effects of adiabatic, relativistic, and quantum electrodynamics interactions on the pair potential and thermophysical properties of helium", *J. Chem. Phys.* **136**, 224303.
- Colclough, A.R., Quinn, T. J., and Chandler, T.R.D., 1979, Acoustic Redetermination of the Gas-Constant, *Proc. R. Soc. London Ser. A* **368**, 125-139
- Coppens, A.B., and Sanders, J.V., 1968, Finite-Amplitude Standing Waves in Rigid-Walled Tubes, *J. Acoust. Soc. Am.*, **43**, 516-529.
- Edwards, G. and Underwood, R., 2011, The electromagnetic fields of a triaxial ellipsoid calculated by modal superposition, *Metrologia* **48**, 114-122.
- Ewing, M.B., McGlashan, M.L., and Trusler, J.P.M. 1986, The Temperature-Jump Effect and the Theory of the Thermal Boundary Layer for a Spherical Resonator. Speeds of Sound in Argon at 273.16K, *Metrologia* **22**, 93-102.
- Ewing, M.B. and Trusler, J.P.M., 2000, Primary acoustic thermometry between T=90 K and T=300 K, *J. Chem. Thermodynam.*, **32**, 1229-1255.
- Gammon, B., 1976, The velocity of sound with derived state properties in helium at -175 to 150 °C with pressure to 150 atm, *J. Chem. Physics* **64**, 2556-2568.
- Garberoglio, G., Moldover, M.R., and Harvey, A.H., 2011, Improved First Principles Calculation of the Third Virial Coefficient of Helium, *J. Res. Natl. Inst. Stand. Technol.* **116**, 729-742.

EDITION 2013

Gavioso, R. M., Benedetto, G., Albo, P. A. G., Ripa, D. M., Merlone, A., Guianvarc'h, C., Moro, F., and Cuccaro, R., 2010a, A determination of the Boltzmann constant from speed of sound measurements in helium at a single thermodynamic state, *Metrologia* **47** 387-409.

Gavioso, R.M., Ripa, D.M., Guianvarc'h, C., Benedetto, G., Giuliano Albo, P.A.G., Cuccaro, R., Pitre, L., and Truong, D. 2010b, Shell Perturbations of an Acoustic Thermometer Determined from Speed of Sound in Gas Mixtures, *Int. J. Thermophysics* **31**, 1739–1748.

Gavioso, R.M., Benedetto, G., Ripa, D.M., Albo, P.A.G., Guianvarc'h, C., Merlone, A., Pitre, L., Truong, D., Moro, F. and Cuccaro, R. 2011, Progress in INRiM Experiment for the Determination of the Boltzmann Constant with a Quasi-spherical Resonator, *Intl. J. Thermophysics* **32**, 1339-1354.

Gillis, K.A., Shinder, I.I., and Moldover, M.R., 2004, Thermoacoustic boundary layers near the liquid-vapor critical point, *Phys. Rev. E* **70**, 021201, 20 pages.

Gillis, K.A. and Moldover, M.R., 1996, Practical determination of gas densities from the speed of sound using square-well potentials, *Int. J. Thermophysics*, **15**, 821-846.

Gillis, K.A., Lin, H., and Moldover, M.R., 2009, Perturbations from Ducts on the Modes of Acoustic Thermometers, *J. Res. Natl. Inst. Stand. Technol.* **114**, 263-285.

Gillis, K.A., 2012, Second-order boundary corrections to the radial acoustic eigenvalues for a spherical cavity, *Metrologia* **49**, L21–L24.

Greenspan, M., 1956, Propagation of Sound in Five Monatomic Gases, *J. Acoust. Soc. Am.*, **28**, 644-648.

Grimsrud D.T., and Werntz, Jr., J.H., 1967, Measurements of the Velocity of Sound in He³ and He⁴ Gas at Low Temperatures with Implications for the Temperature Scale, *Phys. Rev.* **157**, 181-190.

Guianvarc'h, C., Gavioso, R.M., Benedetto, G., Pitre, L., and Bruneau, M., 2009, Characterization of condenser microphones under different environmental conditions for accurate speed of sound measurements with acoustic resonators, *Rev. Sci. Instrum.* **80**, 074901 (10pp).

Hamilton, M. F., Ilinskii, Y. A., and Zabolotskaya, E. A., 2001, Linear and nonlinear frequency shifts in acoustical resonators with varying cross sections, *J. Acoust. Soc. Am.* **110**, 109-119.

Lach, G., Jeziorski, B., and Szalewicz, K., 2004, Radiative Corrections to the Polarizability of Helium, *Phys. Rev. Letters* **92**, 233001.

Lin, H, Gillis, K.A., and Zhang, J. T. 2010, Characterization of Piezoelectric Ceramic Transducer for Accurate Speed-of-Sound Measurement, *Int. J. Thermophysics* **31**, 1234-1247.

Mark D. F., Stuart F. M., and de Podesta M., 2011 New high-precision measurements of the isotopic composition of atmospheric argon. *Geochim. Cosmochim. Acta* **75**, 7494-7501.

May, E. F., Moldover, M. R., and Berg, R. F. 2007, Reference Viscosities of H₂, CH₄, Ar and Xe at Low Densities, *Intl. J. Thermophysics* **28**, 1085-1110.

May, E. F., Pitre, L., Mehl, J. B., Moldover, M. R., and Schmidt, J. W., 2004, Quasi-spherical resonators for metrology based on the relative dielectric permittivity of gases, *Rev. Sci. Instrum.* **75**, 3307-3317.

Mehl, J. B., 2009, Second-order electromagnetic eigenfrequencies of a triaxial ellipsoid, *Metrologia* **46**, 554-559.

Mehl, J. B., 1985, Spherical acoustic resonator: Effects of shell motion, *J. Acoust. Soc. Am.* **78**, 782-788.

EDITION 2013

Mehl, J. B. and Moldover, M. R., 1982, Precondensation phenomena in acoustic measurements, *J. Chem. Phys.* **77**, 455-465.

Mehl, J. B. and Moldover, M. R., 1986, Measurement of the ratio of the speed of sound to the speed of light, *Phys. Rev.* **A34**, 3341-3344.

Mehl, J. B., Moldover, M. R., and Pitre, L., 2004, Designing quasi-spherical resonators for acoustic thermometry, *Metrologia*, **41**, 295-304

Moldover, M. R., Mehl, J. B. and Greenspan, M., 1986, Gas-filled spherical resonators - Theory and experiment, *J. Acoust. Soc. of Am.* **79**, 253-272.

Moldover, M. R., Trusler, J. P. M., Edwards, T. J., Mehl, J. B., and Davis, R. S., 1988, Measurement of the universal gas constant R using a spherical acoustic resonator, *J. of Res. of NBS* **93**, 85-144.

Moldover, M. R., Boyes, S. J., Meyer, C. W., and Goodwin, A. R. H., 1999, Thermodynamic temperatures of the triple points of mercury and gallium and in the interval 217 K to 303 K, *J. Res. Natl. Inst. Standards Technol.* **104**, 11-46.

Moldover, M.R. 2009 Optimizing Acoustic Measurements of the Boltzmann Constant, *Comptes Rendus Physique* **10**, 815-827.

Mook, W. G., editor 2000, "Environmental Isotopes in the Hydrological Cycle: Principles and Applications, Volume I," UNESCO/IAEA Series on Environmental Isotopes in the Hydrological Cycle, available on line at: <http://www.hydrology.nl/ihppublications/149-environmental-isotopes-in-the-hydrological-cycle-principles-and-applications.html>

Pitre, L., Moldover, M.R. and Tew, W.L. 2006, Acoustic Thermometry New Results from 273 K to 77 K and Progress towards 4 K, *Metrologia* **43**, 142-162.

Pitre, L., Sparasci, F., Truong, D., Guillou, A., Risegari, R., and Himbert, M. E., 2011, Measurement of the Boltzmann Constant k_B Using a Quasi-Spherical Acoustic Resonator, *Intl. J. Thermophysics* **32** 1825-1886.

Plumb H., and Cataland, G., 1966, Acoustical Thermometer and the National Bureau of Standards Provisional Temperature Scale 2–20 1965, *Metrologia* **2**, 127-139.

Podobedov, B., 2009, Resistive wall wakefields in the extreme anomalous skin effect regime, *Phys. Rev. Special Topics-Accelerators and Beams* **12**, 044401.

Ripple, D.C., Defibaugh, D.R., Moldover, M.R., and Strouse, G.F., 2003 Techniques for Primary Acoustic Thermometry to 800 K, in "TEMPERATURE: Its Measurement and Control in Science and Industry; Volume VII"; 8th Intl. Temperature Symp., Chicago IL, Oct. 21-24, 2002," edited by D.C. Ripple, pp. 25-30, Am. Institute of Physics.

Ripple, D.C., Strouse, G.F., and Moldover, M.R., 2007, Acoustic Thermometry Results from 271 K to 552 K, *Int. J. Thermophysics* **28**, 1789-1799.

Ripple, D.C., Strouse, G.F., Gillis, K.A., and Moldover, M.R., 2013, Room Temperature Acoustic Transducers for High-Temperature Thermometry, *Proc. 9th Intl. Temperature Symposium, March 19-23, 2012, Anaheim, CA, American Institute of Physics*, (In press).

Rizzo, A., Hätttig, C., Fernández, B., and Koch, H., 2002, The effect of intermolecular interactions on the electric properties of helium and argon. III. Quantum statistical calculations of the dielectric second virial coefficients, *J. Chem. Phys.* **117** 2609-2618.

EDITION 2013

Schmidt, J. W. and Moldover, M. R., 2003, Dielectric Permittivity of Eight Gases Measured with Cross Capacitors, *Int. J. Thermophysics* **24**, 375-403.

Song, S., Yovanovich, M.M., 1987, Correlation of thermal accommodation coefficient for engineering surfaces, in: National Heat Transfer Conference, Pittsburgh, PA, August 9–12, 1987.

Strouse, G. F., Defibaugh, D. R., Moldover, M. R., and Ripple, D. C., 2003, Progress in Primary Acoustic Thermometry at NIST: 273 K to 505 K, in “TEMPERATURE: Its Measurement and Control in Science and Industry; Volume VII; 8th Intl. Temperature Symp. Chicago IL, Oct. 21-24, 2002,” edited by D.C. Ripple, 31-36, AIP Conf. Proc.

Tegeler, Ch., Span, R., and Wagner, W., 1999, A New Equation of State for Argon Covering the Fluid Region for Temperatures From the Melting Line to 700 K at Pressures up to 1000 MPa, *J. Phys. Chem. Ref. Data* **28**, 779-850, as implemented in the computer package: Lemmon, E. W., McLinden, M. O., and Huber, M., L., “REFPROP: Reference Fluid Thermodynamic and Transport Properties,” NIST Standard Reference Database 23, Version 9.0, National Institute of Standards and Technology, Boulder, CO, 2010, <http://www.nist.gov/srd/nist23.cfm>

Trusler, J.P.M. 1991, “Physical Acoustics and Metrology of Fluids”, Taylor and Francis Group, New York, NY and Abington, U. K.

Underwood, R.J., Mehl, J.B., Pitre, L., Edwards, G., Sutton, G., and de Podesta, M., 2010, Waveguide effects on quasispherical microwave cavity resonators, *Meas. Sci. Technol.* **21**, 075103 (11pp)

Underwood, R., Davidson, S., Perkin, M., Morantz, P., Sutton, G., and de Podesta, M., 2012 Pyknetric volume measurement of a quasi-spherical resonator, *Metrologia* **49**, 245-256.

Valkiers, S., Vendelbo, D., Berglund, M., and de Podesta, M., 2010, Preparation of argon Primary Measurement Standards for the calibration of ion current ratios measured in argon, *Int. J. Mass Spectrometry*, **291**, 41-47.

Vogel, E., Jäger, B., Hellmann, R., and Bich, E., 2010, Ab initio pair potential energy curve for the argon atom pair and thermophysical properties for the dilute argon gas. II. Thermophysical properties for low-density argon, *Molecular Physics*, **108**, 3335–3352

Zhang, J.T., Lin, H., Sun, X.J., Feng, K.A., Gillis, K.A., and Moldover, M.R., 2010, Cylindrical Acoustic Resonator for the Re-determination of the Boltzmann Constant, *Intl. J. Thermophysics*, **31**, 1273-1293

Zhang, J.T., Lin, H., Feng, X.J., Sun, J. P., Gillis, K.A., Moldover, M.R., and Duan, Y. Y., 2011, Progress Toward Re-determining the Boltzmann Constant with a Fixed-Path-Length, Cylindrical Resonator, *Intl. J. Thermophysics*, **32**, 1297-1329.